Combustion characterization of waste cooking oil and canola oil based biodiesels under simulated engine conditions

C. Ming[a], I.M. Rizwanul Fattah[a], Qing N. Chan[a,*], Phuong X. Pham[b], Paul R. Medwell[c], Sanghoon Kook[a], Guan H. Yeoh[a], Evatt R. Hawkes[a, d], Assaad R. Masri[b]

[a]*School of Mechanical and Manufacturing Engineering, UNSW Sydney, NSW 2052, Australia*

[b]*School of Aerospace, Mechanical and Mechatronic Engineering, The University of Sydney, NSW 2006, Australia*

[c]*School of Mechanical Engineering, The University of Adelaide, SA 5000, Australia*

[d]*School of Photovoltaic and Renewable Energy Engineering, UNSW Sydney, NSW 2052, Australia*

Abstract

Alternative fuels will come from a variety of feed stocks and refinement processes. Understanding the fundamentals of combustion and pollutants formation processes of these fuels will be useful for their implementation in different combustion systems. In this work, optical diagnostics were performed to waste cooking oil (WCO) and canola oil (CAO) based biodiesel sprays to assess their combustion and soot formation processes. Conventional diesel was used as a reference fuel for comparison with the biodiesels. The experiments were conducted in an optically-accessible constant-volume combustion chamber (CVCC) with simulated compression-ignition engine conditions, with different degree of exhaust gas recirculation. The liquid length and lift-off length results indicate that there was no significant interaction between the liquid phases of the fuels and their combustion regions. The flame lift-off lengths were found to be affected by both the chemical and physical properties of the fuels. It was observed that a larger difference between the lift-off length and the first-luminosity distance

*Corresponding author: qing.chan@unsw.edu.au

March 5, 2018

was correlated with lesser downstream soot formation, although the molecular structure of the fuel was found to affect the process too. Assessing the sooting and combustion characteristics of the biodiesel and diesel flames across the varied ambient O_2 atmospheres revealed that the estimated soot contents of the biodiesel and diesel flames peaked at 15 and 21 vol.% O_2 concentration, respectively. The peak soot contents of the WCO and CAO biodiesel flames were found be comparable, but lower than that of diesel, across the various O_2 environment. The results also demonstrated that the biodiesels have higher normalized peak pressure values than diesel at all O_2 conditions. Two-color pyrometry data demonstrated that the measured soot temperature and soot KL factors of the flames were similar at 15 and 21 vol.% O_2, but varied with further reduction of ambient O_2 concentration. Variations in the combustion duration and flame area were found to be fuel dependent.

Keywords: Biodiesel, Waste cooking oil, Canola oil, Two-color pyrometry

1. Introduction

Diesel-fueled compression-ignition engines are becoming increasingly popular choice for ground transport vehicles because of their high torque output and fuel efficiency. However, particulate emissions from diesel engines, which can profoundly affect human health and environment [1, 2], remain a major concern. Using alternative diesel fuels, such as biodiesels, is widely considered to be a promising method to control particulate emissions from compression-ignition engines during combustion. The oxygen content of biodiesel fuels have been reported to provide an effective route to enhance combustion and to inhibit soot formation in compression-ignition engines [3, 4]. This has motivated many research and development activities, ranging from the modifications of the upstream cultivation process to enhance feedstock production for biofuels [5], down to the detailed study of combustion and emission characteristics of biodiesel fuels in the diesel engines [3, 6] over the past decades. Table 1 presents a summary of selected experimental investigations involving combus-

tion diagnostics of biodiesels in optically-accessible combustion chambers that are relevant to this work, as an example of the quantity of fundamental studies performed in this subject area.

Despite the many previous studies, the impact of the properties of the biodiesel fuels on soot emissions remain only vaguely known due to the multitude and complexity of the associated processes. In addition, biodiesels are mixtures of fatty acid methyl esters (FAMEs) with different chain lengths and degrees of saturation, which can vary significantly depending on their feedstocks [7, 8]. Such variations can have a complicated impact on biodiesel atomization, evaporation, combustion and soot formation processes, and hence, the ensuing engine performance [4, 8]. The lack of control of all of these factors have led to contradictory results being reported in the literature. For instance, many studies have reported that fuels with higher cetane numbers have shorter ignition delays, which would therefore lead to an increased soot formation due to insufficient fuel-ambient mixing before the onset of combustion [9]. Nonetheless, there are other studies that show reduction in soot and unburned hydrocarbon emissions, when fuels of high cetane number values were used [10, 11]. The differences are likely to be attributable to molecular structure effects of the fuels used. In addition, in a previous study conducted by Pham *et al.* [12], it was reported that the oxygen content in biodiesels would contribute towards particle formation suppression in the premixed spray combustion zone, and increased particle oxidization at the flame front. In a separate study that was conducted by Park *et al.* [9], however, it was demonstrated that the soot formation is mainly controlled by the fuel-air mixing process for fuels with similar amount of oxygen within the fuel, and number of carbon-carbon bonds. These findings demonstrate the difficulties in drawing conclusions from a change to a single fuel property, which could simultaneously impact on other fuel properties [13]. The complexities that arise from the inter coupling between the various fuel properties produce some degree of uncertainty as to which effect would have a greater impact on the soot formation process of the flame [14].

Engine operating parameters, such as fuel injection pressure and exhaust

gas recirculation (EGR), can have a pronounced impact on the combustion and pollutant formation processes of the fuel in compression-ignition engines. High pressure fuel injection, for example, could be used to improve spray atomization and combustible mixture preparation, which can lead to reduced particulate emission and improved engine performance [14, 15]. The introduction of EGR can result in low temperature combustion (LTC) condition, which can lead to reduced NOx emissions [16] from compression ignition engines. The effects of these varied operating parameters on the engine and emission performances, however, can also change significantly depending on the fuel type used. For example, it has been reported that increasing injection pressure can potentially lead reduced flame residence time available for fuel elements to undergo soot formation [17], in addition to the general consensus that it can help improve the atomization and vaporisation processes of a fuel. Nonetheless, other studies have also demonstrated that high fuel injection pressure can lead to wall-wetting, which would result in increased engine-out emissions of uHC, CO and smoke [18]. The wall-wetting issue is generally more problematic when biodiesels are used, as they typically have longer spray penetrations due to their higher fuel densities when compared with diesel [19]. In addition, in a previous work that was conducted by Zhang *et al.* [20], it was reported that the effects of EGR may vary depending on the fuels such that a lower oxygen-concentration environment was necessary for diesel to achieve a higher combustion efficiency and lower soot emission, when compared with biodiesels. All these highlight the need to perform a direct assessment the effects of common engine operating parameters on the combustion and pollutant emission processes for the biodiesel fuel of interest, to ensure efficient and clean engine operation when used.

This work is therefore aimed at assessing the combustion properties of biodiesels from the transesterification of waste cooking oil (WCO) and canola oil (CAO) under simulated compression-ignition engine conditions in a constant-volume combustion chamber (CVCC). The WCO biodiesel is specifically targeted as it is the main biodiesel feedstock in Australia [21]. The CAO biodiesel is also selected for study as it has been extensively investigated by the authors

under open flame burner and performance engine settings [12], in addition to having fuel properties that are similar to the WCO biodiesel, and is therefore useful for comparison. Optical diagnostic techniques, including OH chemiluminescence and high-speed flame natural luminosity imaging, are used to assess the impact of these varied parameters both on the air entrainment rate occurring upstream of the lift-off length, and on the downstream soot formation and combustion processes of the biodiesel jet flames. The two-colour pyrometry technique is applied to the recorded flame natural luminosity images to provide soot temperature and concentration information for the jet flames under the test conditions. To provide context to the examination, comparative measurements using a conventional diesel are also performed.

2. Experimental Details

2.1. Constant-volume Combustion Chamber

Experiments were performed in an optically-accessible CVCC under simulated, quiescent diesel engine conditions. The CVCC has a 114×114×114 mm cubical combustion chamber, six window ports, and eight access ports for instrumentations and valves. For this work, sapphire windows were installed at four sides of the chamber to enable optical access. A diesel injector was mounted at the centre of a metal side port so that the fuel spray was directed into the centre of the chamber. An agitator was mounted at the top of the CVCC and was used to maintain a spatially uniform temperature environment. Schematic diagrams of the CVCC configuration along with the diagnostic set-ups used, and the cross-sectional view of the CVCC are shown in Fig. 1. The operation of the chamber was initiated by filling it with a premixed, lean combustible charge (mixture of acetylene, hydrogen, nitrogen and oxygen). The mixture was subsequently ignited with a spark plug to create a high temperature and pressure environment inside the chamber. For this work, an ambient condition with gas density, pressure and temperature of 19.5 kg/m^3, 6 MPa and 1100 K, respectively, was targeted and the fuel injector was triggered once the targeted condition was

reached. The operating conditions were used to match experimental conditions that were selected to ensure that the combustion process of the biodiesels and diesel are fairly complete in previous CVCC studies [20, 22]. The metering of the reactant gases was also controlled so that an environment with 0 or 10, 15 and 21 vol.% O_2 concentration can be generated after the premixed combustion process. The 0 vol.% ambient O_2 concentration (non-reacting) condition was used to provide insights into the liquid length penetration characteristics of the sprays with varied injection schedules, without the complex effects of heat release from the combustion processes. The 10 and 15 vol.% (reacting) ambient O_2 conditions were used, on the other hand, to simulate compression-ignition engine conditions with high and moderate exhaust gas recirculation [23, 24]. The test conditions for the experiments are summarized in Table 2.

The fuel injection system used comprised of a low-pressure fuel pump a high-pressure fuel pump, a Bosch commercial common-rail system (CP4) and an axially drilled single-hole solenoid injector with an orifice diameter of 105 µm. The single-hole injector was used to avoid the complexity that can arise from jet-jet interaction. A common-rail PCV driver (Zenobalti, ZB-1200) was used to regulate and maintain the injection pressure, whilst an injector driver (Zenobalti, ZB-5100) was used to ensure the injection system control the injection duration to deliver the required fuel mass. A summary of the injection conditions used is provided in Table 2.

2.2. Optical Diagnostics

2.2.1. Combustion Diagnostics

A summary of the optical diagnostic techniques and settings used for this work is provided in Table 3. The OH chemiluminescence images were captured using an intensified CCD (ICCD) camera, whilst the flame natural luminosity images were recorded with a high-speed CMOS camera. The cameras were arranged for viewing through the side or bottom windows of the CVCC, as shown in Fig. 1, and were applied simultaneous to image the same injection events. For the OH-chemiluminescence imaging, the light emission from flame

was detected through a 10 nm bandwidth interference filter (centred at 310 nm), using the ICCD camera (Andor iStar) that was fitted with a 50 mm f#3.5 UV lens. The camera was triggered to open for 2.5 ms after the quasi-steady lift-off length of the flame was established, and was closed before the end of injection. The pixel resolution of the image is ∼0.1 mm per pixel. A typical recorded OH-chemiluminescence image is shown in Fig. 2. In this sample image, the injector orifice is located at the left edge of the image, and the WCO biodiesel was injected from left to right at 100 MPa injection pressure and 15 vol.% ambient O_2 concentration.

For the high-speed flame luminosity imaging, a CMOS camera (Photron SA5) equipped with a 85 mm f#1.8 lens that was operated at a frame rate of 15,000 frames per second (fps) was used. The CMOS camera was synchronized to the start of injection of the injector, and 100 images were recorded to ensure that the entire combustion event, from the start of injection till the end of combustion, was captured for each run. A typical instantaneous flame luminosity images captured for the same WCO biodiesel jet flame presented, but at 2.4 ms after start of injection (aSOI), is shown in Fig. 3. The pixel resolution of the image is ∼0.2 mm per pixel. The instantaneous flame luminosity images that were recorded for both CAO biodiesel and diesel flame, under the same experimental conditions, are also presented for comparison purposes. In these images, the fuels were also injected from left to right. It is noted that at least five runs were performed for each measurement to ensure good repeatability.

2.2.2. Spray Diagnostics

Liquid length, which is defined as the maximum distance from the injector tip to liquid fuel penetration for an evaporating fuel spray [25], was measured for each of the fuels to determine the extent of its liquid phase. It is noted that the diffused back illumination (DBI) technique, which has been reported to be more quantitative when compared with other methods because of its built-in reference light intensity [26], was used as the main diagnostic method to obtain liquid length information. For DBI imaging, the collimated light output from

a high-powered, continuous LED that was emitting at a central wavelength of 455 nm, was used for illumination. An engineered diffuser was also placed between the LED light and the spray to ensure homogenized illumination. A high-speed CMOS camera, which was placed directly opposite to the LED light source, was operated at a frame rate of 15,000 frames per second (fps), with 1 µs exposure time and a pixel resolution of ∼0.14 mm per pixel. For the DBI technique, the camera was also synchronized to the start of injection of the injector and 100 images were captured for each run.

To determine the extent of the liquid phase in the DBI images, the light intensity, I, at a pixel location from an image with spray, was compared against the background intensity, I_o, at the same pixel location from an image with no spray. In this work, the calibration of the DBI technique was performed by comparing the DBI images and Mie-scattering images that were recorded using the current experimental setup, for a series of fuel sprays that were subjected to the same set of test conditions. The Mie-scattering images were obtained using the same high-speed camera and high-intensity LED, but with side illumination. The Mie-scattering images obtained were processed using a threshold of intensity that corresponded to 3% of the maximum intensity, following the widely-used Sieber's approach for Mie-scattering post-processing [25, 26]. The cut-off I/I_o value of the DBI images was subsequently determined as 0.3, so that the results of the measurement techniques would match.

2.3. Flame luminosity image post-processing

In this study, a novel color band approach, which was first introduced by Larsson [27] and further explained by Svensson *et al.* [28], was applied to the recorded flame luminosity images, to provide two-dimensional soot temperature and soot distribution information. The color band approach, which only requires the use of a single digital color camera for soot two-color measurements, has the advantage of avoiding errors introduced due to potential misalignment of frames taken by two cameras and eliminates the need for complex optics that are typically required for the more classical implementation of two-color

pyrometry technique. The general theory of two-color thermometry has been described in detail in various papers [27–29], a complete treatment is therefore not provided here. In essence, the signal from an optical detector viewing a radiating soot cloud can be described using Planck's blackbody function that incorporates a wavelength-dependent soot emissivity model, as well as the combined wavelength-dependent responsivity of the detection system used (optics train, filter and high-speed camera). The pixel output, S, when observing soot irradiation at wavelength, λ, can therefore be described as:

$$S_\lambda = \int \epsilon_{soot} \frac{C_1 Q(\lambda)}{\lambda^5 \left[exp\left(\frac{C_2}{\lambda T_{soot}}\right) - 1 \right]} d\lambda. \tag{1}$$

In Eq. 1, $Q(\lambda)$ refers to the optical system response coefficient for each wavelength, C_1 and C_2 are the Planck's first and second constants, respectively, and T_{soot} is the soot temperature. The soot emissivity, ϵ_{soot}, can be modeled with the empirical correlation of Hottel and Broughton [30]:

$$\epsilon_{soot} = 1 - exp(-\frac{KL}{\lambda^\alpha}), \tag{2}$$

where α in Eq. 2 is given as [31]:

$$\alpha = 1.22 - 0.246 \times ln(\lambda). \tag{3}$$

The product KL in Eq. 2 is widely used to characterize the soot content in various combustion systems [28, 29]. From Eq. 1, it can be seen that if the optical response coefficient, $Q(\lambda)$, is known through calibration, S_λ becomes a function of two unknown variables, T_{soot}, and KL. Given that there are two unknowns, any two of the three color channels can therefore be used to produce two equations to solve for T_{soot} and KL. For this work, only signal from the red and green channels were used for the two color calculations, as these two channels have higher signal-to-noise ratios than that of blue (SNRs of 47, 21 and 9 were measured for red, green and blue channels, respectively). The optical response coefficients of the detection system were determined through

calibration using a tungsten filament light source with known spectral emission properties.

2.4. Fuel selection

For this work, two biodiesels (waste cooking oil and canola oil based) possessing long carbon chain lengths, with high unsaturation degrees were studied. Diesel was selected as a reference fuel to be used for comparative studies with these biodiesels. From the fuel specifications data that were provided by the fuel suppliers, both the waste cooking oil (WCO) and canola oil (CAO) based biodiesels have higher cetane number, fuel density, viscosity values when compared with diesel. Both biodiesels have a high degree of unsaturation, as are reflected by their iodine values. For the injection conditions used in this work, the difference in the actual injected mass of the biodiesels and diesel, when measuring with a Bosch tube type injection rate meter, was found to be within experimental errors ($\sim$10%) of the injection rate meter across the varied conditions. The same injection parameters were therefore applied to biodiesels and diesel for all experiments. Gas-chromatography and mass-spectrometry (GCMS) were performed on the biodiesel fuels to determine their chemical compositions. Both WCO and CAO biodiesels are found to comprise mainly of FAMEs with long carbon chains such as oleic, linoleic and linolenic acids, and are oxygenated (11 wt%) leading to their lower heating values and lower stoichiometric mixture fractions than diesel. A summary of the main fuel characteristics of all fuels and main FAME fractions of the biodiesels are provided in Tables 4 and 5, respectively.

3. Results and discussion

3.1. Lift-off length, first-luminosity distance and soot formation distance

Flame structural information, including flame lift-off and first-luminosity distance from the nozzle, during its mixing-controlled combustion phase has been shown to be critical towards the understanding of soot formation process

[32]. The flame lift-off length, which refers to the distance from the fuel injector nozzle to where the flame stabilizes, is indicative of the location where intense combustion reaction of the flame initiates [33], and is widely used to characterize the amount of fuel-air premixing occurring upstream of the lift-off [34]. The first-luminosity distance, on the other hand, refers to the distance from the injector to the location where intense flame luminosity is first detected. The first-luminosity distance is useful to indicate the initial onset of soot, as the natural flame luminosity detected is dominated by soot incandescence in sooty flame. The lift-off lengths of the flames were derived from their time-averaged OH chemiluminescence images, following the approaches that were detailed in Ref. [33]. In brief, the lift-off length value was determined by finding the distance between the injector and first axial location where chemiluminescence intensity of the flame exceeded $\sim$50% of the leveling-off value, as is shown in Fig. 2. The first-luminosity distances, on the other hand, were derived from the high-speed natural flame luminosity images that were captured using the high-speed camera. The images were first corrected for background, dark charge and detector attenuation, and were subsequently binarized to enable logical operations [35, 36]. The first-luminosity distance was determined by measuring the minimum distance from the injector nozzle exit plane to the location where half of the pixels on an arc with a spreading angle of $\theta/2$ are occupied by the binarized flame area. The flame penetration distance was also determined using the same methodology, but is defined as the maximum distance between the injector and the aforementioned arc. These definitions were used to minimize the sensitivity of the first-luminosity distance and flame penetration distance calculations to the threshold settings used or potential fluctuations in the binarized flame area. It is noted that the flame central axis was taken as the line from the injector tip through to the centroid of the flame area, whilst flame spreading angle was defined as the average flame spreading angle between a starting and ending points along the flame central axis. The starting and ending points were set to be 45% and 55% of the instantaneous flame penetration distance.

The average lift-off lengths and the first-luminosity distances of the WCO

and CAO biodiesels and diesel are plotted as functions of injection pressures, for the test conditions with ambient O_2 concentrations of 10, 15 and 21 vol.% in Fig. 4. Dashed lines through the data are included to help the visualization of the trends. Due to the similarity in the trends of the WCO, CAO and diesel data to the effect of ambient O_2 concentration, the data of diesel and CAO under ambient concentration of 10 and 21 vol.% are not shown here. From Fig. 4, it can be seen that lift-off lengths of the flames are found to increase with increasing injection pressure or decreasing ambient O_2 concentration. It is noted that previous studies have shown that an increase in injection pressure would result in higher velocity in spray, which would push the initial combustion zone of the flame downstream [37]. A reduction in ambient O_2 concentration, on the other hand, has been shown to necessitate a greater entrainment of total ambient gas with smaller fraction of oxygen (hence, longer mixing time) before combustion reactions can take place [38]. The current results are therefore consistent with the previously observed trends in lift-off lengths with respect to injection pressure and O_2 concentration effects.

From Fig. 4 it can be observed that the lift-off lengths of the WCO biodiesel flames are consistently longer than those of diesel flames, whilst the lift-off lengths of the CAO biodiesel flames are found to be the lowest amongst the fuels used. Previous studies have demonstrated flame lift-off length is affected by both the chemical and physical properties of the fuel [39]. From Table 4, it can be seen that the cetane number of the WCO biodiesel (*i.e.*, 53.2), albeit slightly higher, is comparable to that of diesel (*i.e.*, 51). Previous studies [13] have noted that there is an inherent uncertainty in the reported cetane number of the fuel, which can be dependent on the measurement methodology and testing facility used. The ambient conditions used for cetane number measurements are also significantly different to the experimental conditions of this work. Therefore, to eliminate the potential ambiguity of the cetane number rating and the actual ignition delay, the light-based ignition delay of the fuels, when injected at a baseline injection pressure of 100 MPa, were assessed. From the measurement results, the ignition delays for the biodiesel and diesel fuel jets were found to

be 0.6, 0.4 and 0.33±0.06 ms at ambient oxygen conditions of 10, 15 and 21% O_2 concentrations, respectively. The ignition delays of the fuels are observed to follow the expected trend of decreasing ignition delay with increasing ambient gas oxygen concentration. The invariant ignition delay values measured for the fuels, however, do not match their lift-off length trend. It is noted that whilst the ignition characteristic of a fuel is generally expected to affect its lift-off behavior, such that a fuel with smaller ignition delay would display shorter lift-off, many previous studies [13, 40, 41] have reported difficulty in observing such one-to-one correlation between the lift-off length and the fuel ignition characteristic. Whilst the exact reason behind this discrepancy in trends is still unclear, but there is some evidence that several other factors, such as first-stage cool flame activity [13, 41], can potentially affect the lift-off behavior of the fuel. It is worth noting, however, the viscosity of the WCO biodiesel is greater than that of diesel, which can impact on the extent of the atomization, vaporization and fuel-air mixing processes of the fuel. The higher heat of vaporization value, which could be attributed to the presence of FAMEs with longer carbon chains [25] in the biodiesel, would affect the vaporization and fuel-air mixing processes. All these can lead to a prolonged time between the beginning of fuel injection and the start of combustion process that would subsequently impact the ignition quality of the WCO biodiesel fuel. In the case of the CAO biodiesel, however, the cetane number of the CAO biodiesel (*i.e.*, 59), however, is comparatively higher than both WCO biodiesel and diesel. The higher chemical reactivity of the CAO biodiesel would therefore weaken the effect of delay that can arise from its physical properties on the auto-ignition process. The liquid lengths of the WCO and CAO biodiesels were also measured and were found to be ∼8.7 mm and ∼8.6 mm, respectively, which are longer than that of diesel (∼7.7 mm). The liquid lengths of all fuels were, nonetheless, noted to be shorter than their lift-off lengths, suggesting that there was no significant interplay between the spray and combustion processes for the fuels under the test conditions of this work.

From Fig. 4, it can also be seen that the first-luminosity distances of

biodiesels and diesel increase with increasing injection pressure or decreasing ambient O_2 concentration. The first-luminosity distance values are also consistently greater than the corresponding lift-off lengths of the jet flames. The finding is consistent with the observations of previous studies [32, 34] that have reported that the soot precursors, which are the foundation for soot growth downstream, occurred from the partially premixed fuel-rich combustion zone upstream. From the figure, it can also be seen that the first-luminosity distances, and hence, the soot inception locations, of both WCO and CAO biodiesels are located downstream to that of diesel. As is noted in previous studies [34], once soot is formed, the soot can be transported from the soot formation and growth regions into the flame boundary or tip regions, where soot oxidation reactions would occur [34]. It is noted that the maximum flame penetration distances that are determined from the average of the instantaneous flame luminosity images, such as shown in Fig. 3, recorded at injection timings just prior to the end of injections for the biodiesel fuels are similar or shorter than that of diesel at all conditions. It can therefore be anticipated that the soot formed in the biodiesel flames would have less residence time for soot formation and growth processes, prior to soot oxidation, when compared with diesel flame.

In previous studies, it has been shown the soot inception time of a jet flame can be approximated from the observed location of the first-luminosity formation relative to the flame lift-off [34]. This distance of lift-off length to soot formation region, which is termed as soot formation distance in the subsequent discussion, has been shown to depend strongly on fuel type, such that a longer distance is observed for a fuel with lower soot formation tendency [32, 34]. In Fig. 5, the soot formation distances of the WCO biodiesel, CAO biodiesel and diesel jet flames are plotted as functions of the ambient O_2 concentrations. The peak spatially integrated natural luminosity (SINL) values of the biodiesel and diesel flames under different test conditions are also computed and are presented in Fig. 5. It is acknowledged that the SINL signal, which is calculated by summing up the intensities of all pixels of each image, is a complex function of the soot concentration, properties, flame area and temperature [42]. Nonetheless,

the peak SINL has been widely demonstrated to be useful in providing a relative measure of the soot content of sooty flames, and is therefore used here to rank-order the soot level of the flames.

In Fig. 5, it can be seen that under the same test and injection conditions, the soot formation distances of the biodiesel flames are consistently longer than that of diesel. As discussed in previous studies (*e.g.*, [32]), the progression of soot formation downstream to the lift-off length is complex, and is dependent upon mixture stoichiometry, original molecular structure, local mixture temperature and residence time. The combined fuel oxygenation, molecular structure and fuel composition effects of the biodiesels would therefore contribute towards their observed longer soot formation distance when compared with diesel. From Fig. 5, it can be seen that a higher peak SINL value/soot content is observed for flame with shorter soot formation distance. As discussed in previous studies [32], a longer soot formation distance implies that more residence time is required before soot inception or any subsequent soot growth can occur. During this time, the continual entrainment and mixing of ambient O_2 and hot combustion products from the surrounding and diffusion flame could contribute to the suppression of the total soot growth, and hence, the soot content within the flames [32].

From Fig. 5, it can be seen that the biodiesel and diesel flames display different characteristics across the varied ambient O_2 concentrations. Specifically, the soot formation distance of diesel is found to decrease monotonically with increasing ambient O_2 concentration. The soot formation distance of the biodiesels, on the other hand, is observed to first decrease and then increase as the ambient O_2 concentration increases from 10 to 21 vol.%. As is noted in the previous studies [43], at lower ambient O_2 concentration, an increase in the entrainment of ambient gases into the flame would occur to compensate for the reduction in O_2 concentration. Such increase in gas entrainment would result in a lowering of flame temperature and hence, reaction rate, as there would be more inert gases to be heated up within the flame. The dilution effect would therefore also slow down the soot formation and oxidation processes, resulting in less net soot

generation. The impact of reduced ambient O_2 concentration, however, have been reported in several previous studies to be less significant for biodiesels than diesel. For example, Mayo *et al.* [39] observed that soybean biodiesel maintained a higher high-temperature reactivity than diesel under reduced O_2 concentrations. In their study, they attributed their results to the fuel oxygen availability in their biodiesel fuel. It is noted that similar observations were also made in an experimental study that was performed by Zhang *et al.* [20], such that the SINL values of the waste cooking oil biodiesel and diesel flames were observed peaked at O_2 concentrations of 15 and 21 vol.%., respectively, when the ambient O_2 concentration was varied from 12 to 21 vol.%. In their study, it was suggested that under the ambient O_2 concentration of 15 vol.% and a bulk temperature of 1000 K, the soot formation process of the biodiesel flame may have been maintained without sufficient oxidation, which resulted in the increased soot yield observed.

A closer inspection of the combustion characteristics of the biodiesels in Fig. 5 reveals that, for the test conditions of this study, the soot formation distances of the CAO biodiesel flames are consistently longer than that of the WCO biodiesel flames. This is despite the CAO biodiesel flames having shorter lift-off lengths (see Fig. 4) and would therefore experience less air entrainment prior to the initial combustion zone (*i.e.*, upstream of lift-off length). In addition, despite the differences in the soot formation distances of the biodiesel flames, the peak soot content of the flames were still found to be comparable. These findings therefore imply that there are other factors that have impacted on the soot formation process, other than fuel-air mixing. In a recent study that was presented by Park *et al.* [9] involving various oxygenated fuels, it has been demonstrated that the fuel molecular structure would strongly affect the soot formation process of the flame, in addition to fuel-air mixing. From Table 4, it can be seen that whilst the biodiesels are similar in terms of the values of their oxygen content and stoichiometry air to fuel ratios, the CAO biodiesel has a slightly longer average carbon chain length (a lower saponification number implies longer chain length [12]) than WCO biodiesel. Previous studies have

shown that the chain length is inversely correlated to the ignition delay, such that a longer chain length would contribute towards decreased ignition delay (*i.e.* higher cetane number), and hence, a lesser fraction of premixed combustion for the flame. From Table 4, it can also be seen that the CAO biodiesel has a slightly lower degree of unsaturation, when compared with the WCO biodiesel. It is noted that iodine number is a measure of the mass of iodine consumed per 100 g of fatty acids, such that a unit of iodine number would indicate the presence of a mole of carbon double bond per 100 moles of fatty acids with an average molecular weight of 280 g/mol. Given that previous studies have demonstrated that there is a correlation between unsaturated FAME content in biodiesel and the amount of soot-precursor-generating species produced during combustion [44, 45], a lower degree of unsaturation would result in lesser soot propensity for the flame. Together, these findings again highlight the total soot contents of the flames are affected by the combined effects of fuel-air mixing and molecular structures on the soot formation and oxidation processes [46], and the challenges in determining which effect is more significant on the soot processes.

For further insights into the combustion characteristics of the fuels under varied O_2 concentration conditions, the normalized peak pressure (NPP) values were calculated [43, 46] to provide heat release information of the fuels . The NPP value measured during the combustion has been demonstrated to be reflective of the actual thermal potential of the fuel under the test condition and experimental equipment, and can be estimated using:

$$NPP = \frac{p_f}{p_r} \times \frac{E_r}{E_f}, \tag{4}$$

where p_f and p_r refer to the peak pressures of the tested and reference fuels. The energy input values of the tested and reference fuels, which are represented using E_f and E_r, can be calculated using $E = \rho V Q_{LHV}$. The NPP values of the WCO, CAO biodiesels and diesel, which were injected at a fixed injection pressure of 100 MPa, into ambient conditions with O_2 concentrations of 10, 15

and 21 vol.%, respectively, are presented in Fig. 6. Diesel, injecting into an ambient environment with 21 vol.% O_2 concentration at an injection pressure of 100 MPa, is used as the reference fuel for the plot. From the figure, it can be seen that the biodiesels have larger NPP values, and therefore higher thermal efficiencies than that of diesel, across the varied ambient O_2 conditions. In addition, it can also be seen that the NPP values of the biodiesels are found to be slightly higher at an ambient condition of 15 vol.% O_2, whereas the NPP value of the diesel is observed to peak at 21 vol.% O_2. The NPP values of all fuels, however, were found to be at their lowest at 10 vol.% O_2. It is noted a similar observation is also reported in a previous study by Liu *et al.* [43] to examine the combustion characteristics and soot distributions of butanol and soybean biodiesel fuels under varied ambient O_2 concentration conditions (from 21 to 10 vol.%.) but at a fixed ambient temperature of 1000 K. In their study, it was found that the highest heat release values were measured, when the fuels were subjected to an ambient condition with O_2 concentration of 16 vol.%. The fuels were also observed to have the lowest pressure rise values when subjected to an ambient O_2 concentration of 10.5 vol.%, which were attributed to the occurrence of incomplete combustion at low O_2 concentration. It is noted that previous studies have indicated that the combustion process of diesel is more affected by reduced oxygen atmospheres, when compared with biodiesels, as diesel does not contain fuel oxygen [39, 47]. In addition, the reaction rates of the aromatic compounds that are available in the diesel, but not biodiesels, have been reported to be sensitive towards oxygen reduction, which can subsequently reduce the reactivity of the diesel fuel. All these would contribute towards the varying NPP trends of the biodiesel and diesel fuels across the varied ambient O_2 conditions. Further investigation, however, is required to elucidate the current results.

3.2. Soot temperature and soot KL factor

As is noted in the previous section and other studies [14, 48], the natural luminosity of a flame is a function of the local soot concentration and tempera-

ture. The temporal evolution of average soot temperature and soot KL factor of the flames, under varied ambient O_2 conditions (10, 15 and 21 vol.%), but at a fixed injection pressure of 100 MPa, are therefore plotted to provide additional insights. It should be noted that the two-color pyrometry technique is a line-of-sight method and therefore, its accuracy is susceptible to the spatial gradients in soot properties within the measurement volume, along the optical path. The technique has been previously reported to have a temperature uncertainty range of $\sim$150 K, and is only reliable for the qualitative soot concentration comparison [28]. Typical instantaneous soot temperature and KL factor fields at three time instances, which were generated using the two-color pyrometry methodology for the WCO biodiesel jet flame at the condition of 15 vol.% O_2 concentration, are presented in Fig. 7. In these images, the injector tip is located at the top of the images, and the time instances were selected to cover the period from the initial to the quasi-steady stage of the spray combustion event. The average soot temperature and soot KL factor values for all fuels, which correspond to the average values of all pixels in the two-color image frame at each time instant, are presented in Fig. 8. The average soot temperature and KL factor values are presented from the start of soot emergence until the end of soot detection. From the figure, it can be seen that the measured soot temperature and soot KL factors increase rapidly to reach quasi-steady values during the stabilized periods of their injections. The trends of the plots during the quasi-steady periods are found to be similar for the fuels, with the highest and lowest soot temperature values observed for the 21 vol.% and 10 vol.% O_2 cases, respectively. The soot KL factor of the fuels is also observed to display similar characteristics, such that the highest and lowest values are found for the 21 vol.% and 10 vol.% cases, respectively. It is noted that the comparatively lower soot temperature and soot KL factor values of the flames at 10 vol.% case imply that the low O_2 condition has affected the combustion processes of the flames [43]. It is noted that the soot temperature and KL factor values measured are sensitive to the experimental conditions and settings used. It is therefore not possible to directly compare the current measurement with previous studies. The observed values, however,

are broadly consistent to those measured for WCO flames flame with similar arrangement, as measured by Zhang *et al.* [22].

From Fig. 8, it can be observed that the overall characteristics of the average soot temperature and soot KL factor profiles of the fuels are comparable. For both the average soot temperature and KL factor plots, it can be seen that the time that is taken for the flames to reach their maximum quasi-steady values increases with decreasing ambient O_2 concentration. Similarly, the combustion periods of the flames are also observed to increase with decreasing O_2 level, which is to be expected, as more mixing would be required for complete combustion to occur under diluted conditions [49]. It is noted, however, that the combustion duration of the diesel flame is similar to that of the biodiesel flames for the 21 vol.% case, but becomes comparatively longer at lower ambient O_2 concentration. The average soot temperature and soot KL factor values of the flames increase after the quasi-steady periods (*i.e.*, after the end of injection at ∼2.68 ms aSOI). It is noted that recent work [50, 51] have demonstrated that after the end of injection, the entrainment of ambient gases into the jet can increase significantly to change the soot formation and oxidation processes. scale=0.8 soot temperature and soot KL factor could therefore be potentially attributed to the occurrence of enhanced soot oxidation in the low soot temperature and KL zones, leaving the average temperature and soot KL factor to be dominated by the soot signal from the local high temperature and soot concentration regions [29]. Focusing on quasi-steady periods for the flames, prior to the end of injection, it can be seen that a decrease in the ambient O_2 condition did not appear to significantly impact on the average soot temperature and soot KL factor values of the flames, until it was reduced to 10 vol.% O_2. This, combined with the reduced NPP values observed for the fuels at 10 vol.% O_2 concentration in Fig. 6, indicate that the combustion processes of the flames were significantly affected for the 10 vol.% O_2 cases.

From the figure, it can be seen that the average soot temperature and KL factor values of the biodiesel flames are comparable (within the uncertainties of the technique) at all ambient conditions. The average soot temperature and KL

factor values of the diesel, on the other hand, are observed to be similar to the biodiesels for the 21 and 15 vol.% cases, but the average soot KL factor of the diesel flame become lower than that of the biodiesels at 10 vol.% O_2 concentration. To provide further insights, the trends of the average soot KL factors are also compared with the corresponding integrated soot KL factors over the soot areas of the flames, whihc are shown in Fig. 9. From Fig 9, the integrated soot KL factor value of the diesel flame, which is representative of the total soot [22], is found to be higher than the biodiesels at 21 vol.% O_2 concentration. The differences in the integrated soot KL factor values between the diesel and biodiesel flames, however, reduce with decreasing ambient O_2 concentration, such that the diesel flame is observed to have the lowest integrated soot KL factor value for at 10 vol.% O_2 concentration. Taken together, the results indicate that the soot area of the diesel flame is largest amongst the flames at 21 vol.% O_2, but the differences gradually reduce with decreasing O_2 concentration. It can also be deduced that the biodiesel flames displayed lesser variation in soot areas with changing ambient O_2 concentration, which is consistent with the previous finding that the combustion process of biodiesel is less affected by reduced oxygen atmospheres when compared with diesel.

4. Conclusion

To study the combustion characteristics of biodiesel under compression-ignition experiments, a set of optical diagnostics have been applied to waste cooking oil (WCO) and canola oil (CAO) biodiesels. Diesel was used as reference fuel for comparative studies with the biodiesels. Experiments were performed in an optically-accessible constant-volume combustion chamber (CVCC) at ambient conditions that are representative of compression-ignition engine (19.4 kg/m^3 ambient density, 1100 K bulk temperature, 10-21 vol.% ambient O_2 concentrations, 70-130 MPa injection pressures). The liquid lengths of the biodiesels were also measured, and were found to be longer than that of diesel, under the test conditions of this work. The liquid lengths of all fuels were

measured to be shorter than the corresponding lift-off lengths of the flames, therefore implying that significant interaction between the spray and combustion processes of the fuels was not at play. The results revealed that for the investigated experimental conditions, the lift-off lengths were affected by both the chemical and physical properties of the fuels. In addition, a general trend was also observed for the soot content of the flames, such that a larger difference between the lift-off length and the first-luminosity distance, was found to correlate with lesser downstream soot production. Assessing the sooting and combustion characteristics of the biodiesel and diesel flames across the varied ambient O_2 concentration, the estimated soot content of the biodiesel flames were found to be comparable with each other, but lower than that observed for diesel. The estimated soot contents of the biodiesel and diesel flames were also observed to reach their maxima at 15 and 21 vol.% O_2 concentration, respectively. The normalized peak pressure (NPP) values, and therefore, the thermal efficiencies of the biodiesels, on the other hand, were measured to be higher than that of diesel. From the two-color measurement results, it can be seen a decrease in the ambient O_2 condition did not appear to significantly impact on the average soot temperature and soot KL factor values of the flames, until it was reduced to 10 vol.% O_2. The combustion durations of the biodiesel flames were observed to be similar to that of diesel at 21 vol.%, but became comparatively shorter once the ambient O_2 concentration was reduced to 15 vol.%. The combustion durations of all flames were found to be prolonged significantly, when the ambient O_2 concentration was further reduced to 10 vol.%. The change in the soot areas of the biodiesel flames with varied O_2 concentration atmosphere were found to be less significant than that of the diesel flame.

Acknowledgments

The authors wish to acknowledge the financial support of Australia Research Council (ARC) and an Australian Academy of Technological Sciences and Engineering (ATSE) Priming Grant.

References

[1] J. S. Lighty, J. M. Veranth, A. F. Sarofim, Combustion aerosols: Factors governing their size and composition and implications to human health, Journal of the Air & Waste Management Association 50 (2000) 1565–1618.

[2] V. Ramanathan, G. Carmichael, Global and regional climate changes due to black carbon, Nature Geoscience 1 (2008) 221–227.

[3] R. L. McCormick, M. S. Graboski, T. L. Alleman, A. M. Herring, K. S. Tyson, Impact of biodiesel source material and chemical structure on emissions of criteria pollutants from a heavy-duty engine, Environmental Science & Technology 35 (2001) 1742–1747.

[4] X. Wang, Z. Huang, O. A. Kuti, W. Zhang, K. Nishida, An experimental investigation on spray, ignition and combustion characteristics of biodiesels, Proceedings of the Combustion Institute 33 (2011) 2071–2077.

[5] A. Dash, R. Banerjee, Enhanced biodiesel production through phyco-myco co-cultivation of Chlorella minutissima and Aspergillus awamori: An integrated approach, Bioresource Technology 238 (2017) 502–509.

[6] R. L. McCormick, J. D. Ross, M. S. Graboski, Effect of several oxygenates on regulated emissions from heavy-duty diesel engines, Environmental Science & Technology 31 (1997) 1144–1150.

[7] C. J. Chuck, C. D. Bannister, J. G. Hawley, M. G. Davidson, I. L. Bruna, A. Paine, Predictive model to assess the molecular structure of biodiesel fuel, Energy & Fuels 23 (2009) 2290–2294.

[8] S. K. Hoekman, A. Broch, C. Robbins, E. Ceniceros, M. Natarajan, Review of biodiesel composition, properties, and specifications, Renewable and Sustainable Energy Reviews 16 (2012) 143 – 169.

[9] W. Park, S. Park, R. D. Reitz, E. Kurtz, The effect of oxygenated fuel properties on diesel spray combustion and soot formation, Combustion and Flame 180 (2017) 276–283.

[10] D. Karonis, E. Lois, S. Stournas, F. Zannikos, Correlations of exhaust emissions from a diesel engine with diesel fuel properties, Energy & Fuels 12 (1998) 230–238.

[11] R. Nishiumi, A. Yasuda, Y. Tsukasaki, T. Tanaka, Effects of cetane number and distillation characteristics of paraffinic diesel fuels on PM emission from a DI diesel engine, SAE paper (2004) 2004–01–2960.

[12] X. P. Pham, Influences of molecular profiles of biodiesels on atomization, combustion and emission characteristics, Ph.D. thesis, School of Aerospace, Mechanical and Mechatronic Engineering, The University of Sydney (2015).

[13] S. Kook, L. M. Pickett, Soot volume fraction and morphology of conventional, Fischer-Tropsch, coal-derived, and surrogate fuel at diesel conditions, SAE International Journal of Fuels and Lubricants 5 (2012) 647–664.

[14] X. Wang, O. A. Kuti, W. Zhang, K. Nishida, Z. Huang, Effect of injection pressure on flame and soot characteristics of the biodiesel fuel spray, Combustion Science and Technology 182 (2010) 1369–1390.

[15] L. G. Dodge, S. Simescu, G. D. Neely, M. J. Maymar, D. W. Dickey, C. L. Savonen, Effect of small holes and high injection pressures on diesel engine combustion., SAE Paper (2002) 2002–01–0494.

[16] Y. Wu, R. Huang, C. F. Lee, C. Huang, Effects of the exhaust gas recirculation rate and ambient gas temperature on the spray and combustion characteristics of soybean biodiesel and diesel, Proceedings of the Institution of Mechanical Engineers, Part D: Journal of Automobile Engineering 226 (2012) 372–384.

[17] L. M. Pickett, D. L. Siebers, Soot in diesel fuel jets: effects of ambient temperature, ambient density, and injection pressure, Combustion and Flame 138 (2004) 114 – 135.

[18] C. Woo, S. Kook, E. R. Hawkes, Effect of intake air temperature and common-rail pressure on ethanol combustion in a single-cylinder light-duty diesel engine, Fuel 180 (2016) 9–19.

[19] S. H. Yoon, C. S. Lee, Effect of biofuels combustion on the nanoparticle and emission characteristics of a common-rail DI diesel engine, Fuel 90 (2011) 3071–3077.

[20] J. Zhang, W. Jing, W. Roberts, T. Fang, Soot temperature and KL factor for biodiesel and diesel spray combustion in a constant volume combustion chamber, Applied Energy 107 (2013) 5265.

[21] Biofuels Associate of Australia, Biodiesel in Australia, http://biofuelsassociation.com.au/biofuels/biodiesel/biodiesel-in-australia/ [Accessed: 14th Feb 2018] (2018).

[22] J. Zhang, W. Jing, W. L. Roberts, T. Fang, Soot measurements for diesel and biodiesel spray combustion under high temperature highly diluted ambient conditions, Fuel 135 (2014) 340 – 351.

[23] W. Jing, W. L. Roberts, T. Fang, Spray combustion of Jet-A and diesel fuels in a constant volume combustion chamber, Energy Conversion and Management 89 (2015) 525–540.

[24] V. L. Stringer, W. L. Cheng, C.-F. F. Lee, A. C. Hansen, Combustion and emissions of biodiesel and diesel fuels in direct injection compression ignition engines using multiple injection strategies, SAE paper (2008) 2008–01–1388.

[25] D. Siebers, Liquid-phase fuel penetration in diesel sprays, SAE paper (1998) 980809.

[26] L. M. Pickett, C. L. Genzale, J. Manin, Uncertainty quatification for liquid penetration of evaporating sprays at diesel-like conditions, Atomization and Sprays 25 (2015) 425–452.

[27] A. Larsson, Optical studies in a DI diesel engine, SAE paper (1999) 1999–01–3650.

[28] K. I. Svensson, A. J. Mackrory, M. J. Richards, D. R. Tree, Calibration of an RGB, CCD camera and interpretation of its two-color images for KL and temperature, SAE paper (2005) 2005–01–0648.

[29] K. Zha, R. Florea, M. Jansons, Soot evolution with cyclic crank-angle-resolved two-color thermometry in an optical Diesel engine fueled with biodiesel blend and ULSD., Jounral of Engineering for Gas Turbines and Power 134 (2012) 092803–092803–7.

[30] H. C. Hottel, F. P. Broughton, Determination of true temperature and total radition from luminous gas flames, Industrial & Engineering Chemistry Analytical Edition 4 (1932) 166–175.

[31] S. Singh, R. D. Reitz, M. R. B. Musculus, 2-color thermometry experiments and high-speed imaging of multi-mode diesel engine combustion, SAE paper (2005) 2005–01–3842.

[32] J.-G. Nerva, C. L. Genzale, S. Kook, J. M. García-Oliver, L. M. Pickett, Fundamental spray and combustion measurements of soy methyl-ester biodiesel, International Journal of Engine Research 14 (2013) 373–390.

[33] B. Higgins, D. Siebers, Measurement of the flame lift-off location on DI diesel sprays using OH chemiluminescence, SAE paper (2001) 2001–01–0918.

[34] L. M. Pickett, D. L. Siebers, Soot formation in Diesel fuel jets near the lift-off length, International Journal of Engine Research 7 (2006) 103–130.

[35] Q. N. Chan, P. R. Medwell, G. J. Nathan, Algorithm for soot sheet quantification in a piloted turbulent jet non-premixed natural gas flame, Experiments in Fluids 55 (2014) 1827.

[36] N. H. Qamar, Z. T. Alwahabi, G. J. Nathan, Q. N. Chan, Soot sheet dimensions in turbulent nonpremixed flames, Combustion and Flame 158 (2011) 2458–2464.

[37] D. Siebers, B. Higgins, Flame lift-off on direct-injection Diesel sprays under quiescent conditions, SAE paper (2001) 2001–01–0530.

[38] D. Siebers, B. Higgins, L. Pickett, Flame lift-off on direct-injection Diesel fuel jets: Oxygen concentration eEffects, SAE paper (2002) 2002–01–0890.

[39] M. P. Mayo, A. L. Boehman, Ignition behavior of biodiesel and diesel under reduced oxygen atmospheres, Energy & Fuels 29 (2015) 6793–6803.

[40] L. M. Pickett, D. L. Siebers, Fuel effects on soot processes of fuel jets at DI diesel conditions, SAE Paper (2003) 2003–01–3080.

[41] L. M. Pickett, D. L. Siebers, C. A. Idicheria, Relationship between ignition processes and the lift-off length of Diesel fuel jets, SAE Paper (2005) 2005–01–3843.

[42] C. J. Polonowski, C. J. Mueller, C. R. Gehrke, T. Bazyn, G. C. Martin, P. M. Lillo, An experimental investigation of low-soot and soot-free combustion strategies in a heavy-duty, single-cylinder, direct-injection, optical diesel engine, SAE International Journal of Fuels and Lubricants 5 (2011) 51–77.

[43] H. Liu, C.-f. F. Lee, M. Huo, M. Yao, Combustion characteristics and soot distributions of neat butanol and neat soybean biodiesel, Energy & Fuels 25 (2011) 3192–3203.

[44] S. M. Sarathy, S. Gaïl, S. A. Syed, M. J. Thomson, P. Dagaut, A comparison of saturated and unsaturated C_4 fatty acid methyl esters in an opposed flow diffusion flame and a jet stirred reactor, Proceedings of the Combustion Institute 31 (2007) 1015–1022.

[45] Z. Wang, L. Li, J. Wang, R. D. Reitz, Effect of biodiesel saturation on soot formation in diesel engines, Fuel 175 (2016) 240–248.

[46] H. Liu, M. Huo, Y. Liu, X. Wang, H. Wang, M. Yao, C.-f. F. Lee, Time-resolved spray, flame, soot quantitative measurement fueling n-butanol and soybean biodiesel in a constant volume chamber under various ambient temperatures, Fuel 133 (2014) 317–325.

[47] A. S. E. Cheng, A. Upatnieks, C. J. Mueller, Investigation of fuel effects on dilute, mixing-controlled combustion in an optical direct-injection Diesel engine, Energy & Fuels 21 (2007) 1989–2002.

[48] H. Zhao, N. Ladommatos, Optical diagnostics for soot and temperature measurements in diesel engines, Progress in Energy and Combustion Science 24 (1998) 221–255.

[49] W. Jing, W. L. Roberts, T. Fang, Effects of ambient temperature and oxygen concentration on diesel spray combustion using a single-nozzle injector in a constant volume combustion chamber, Combustion Science and Technology 185 (2013) 1378–1399.

[50] M. Musculus, T. Lachaux, L. Pickett, C. Idicheria, End-of-injection over-mixing and unburned hydrocarbon emissions in low-temperature-combustion diesel engines, SAE paper (2007) 2007–01–0907.

[51] M. Musculus, K. Kattke, Entrainment waves in diesel jets, SAE paper (2009) 2009–01–1355.

[52] X. Wang, Z. Huang, W. Zhang, O. A. Kuti, K. Nishida, Effects of ultra-high injection pressure and micro-hole nozzle on flame structure and soot formation of impinging diesel spray, Applied Energy 88 (2011) 1620–1628.

Fuels	Combustion ambient test conditions	Injection specifications	Reference
Diesel, JP-8, world average Jet A blend, Fischer-Tropsch fuel, coal-derived fuel, surrogate fuel	6-6.7 MPa 900-1000 K, 15% O_2 concentration	Single-hole 0.09 mm hole diameter 150 MPa injection pressure	[13]
Butanol, soybean biodiesel	3.3-4.2 MPa, 800-1000 K, 21% O_2 concentration,	Six hole, 0.145 mm hole diameter, 134 MPa injection pressure	[43]
Diesel, soybean biodiesel, ethanol, n-butanol	2.9-4.2 MPa, 700-1000 K, 21% O_2 concentration,	Six hole, 0.145 mm hole diameter, 134 MPa injection pressure	[46]
Diesel, soybean biodiesel	2 MPa, 873 K, 9.6-20.8% O_2 concentration	Six hole, 0.1 mm hole diameter, 100 MPa injection pressure	[39]
Diesel, soy methyl ester	6-6.7 MPa, 900-1000 K, 15% O_2 concentration,	Single-hole, 0.9 mm hole diameter, 150 MPa injection pressure	[32]
JIS# Diesel, palm oil biodiesel, cooking oil biodiesel	4 MPa, 885 K, 21% O_2 concentration	Single-hole, 0.16 mm hole diameter 100-300 MPa injection pressure	[14, 52]
Diesel, soybean biodiesel	2 MPa, 800-1200 K, 15-21% O_2 concentration	Six hole, 0.145 mm hole diameter, 100 MPa injection pressure	[16]
Diesel, waste cooking oil biodiesel	3.5-5.3 MPa, 800-1200 K, 21% O_2 concentration	Six hole, 0.152 mm hole diameter, 100 MPa injection pressure	[20, 22]

Table 1: Summary of selected experimental conditions involving investigations of biodiesels in combustion chambers cited in this work.

Test conditions	
Oxygen level (vol.%)	0 (non-reacting), 10, 15, 21 (reacting)
Ambient density (kg/m^3)	19.5
Pressure (MPa)	6
Bulk temperature at injection (K)	1100
Injection conditions	
Nozzle diameter (µm)	105
Injection pressure (MPa)	70, 100, 130
Injection duration (ms)	2.68

Table 2: Summary of test and injection conditions.

Diagnostic techniques	OH chemiluminescence imaging	High-speed flame luminosity imaging	Diffused back illumination
Camera	Intensified CCD camera (Andor iStar)	High-speed CMOS camera (Photron SA5)	
Frame rate (frames per second)	-	15,000	
f-number	3.5	1.8	1.8
Pixel resolution (mm per pixel)	0.1	0.2	0.14

Table 3: Combustion and spray imaging setup.

Main fuel characteristics			
	WCO	CAO	D
Saponification number	193	188	-
Cetane number	53	59	51
Viscosity @ 293 K, (mm^2/s)	4.6	4.65	3.2
Oxygen content (wt%)	10.8	11	0
Lower HV (MJ/kg)	38.5	35.8	41.1
Stoichiometry air-fuel-ratio (AFR) by mass	12.7	12.5	14.5
Iodine number	95	94	-

Table 4: Main fuel characteristics of waste cooking oil (WCO), canola oil (CAO) based biodiesels and diesel (D).

Main FAMEs (vol%)		
	WCO	CAO
Myristic, C14:0	0.79	-
Palmitic, C16:0	15.42	3.94
Stearic, C18:0	6.13	2.24
Oleic, C18:1	45.64	64.07
Linoleic, C18:2	28.63	18.93
Linolenic, C18:3	3.39	9.15
Eicosanoic, C20:0	-	0.45
Eicosenoic, C20:1	-	1.22

Table 5: Main fatty acid methyl esters (FAMEs) of (in vol.%) the waste cooking oil (WCO) and canola oil (CAO) based biodiesels.

List of Figures

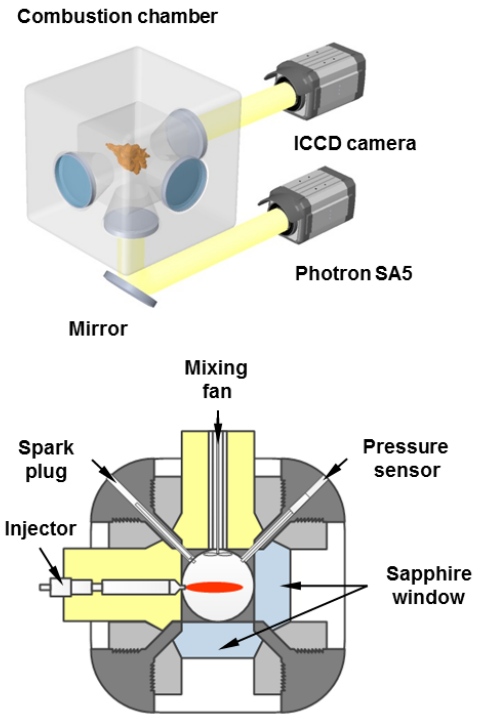

Figure 1: Schematic diagrams of the experimental arrangement used, including the combustion vessel, OH-chemiluminescence and high-speed natural luminosity imaging setups (top) and the cross-sectional view of the chamber (bottom).

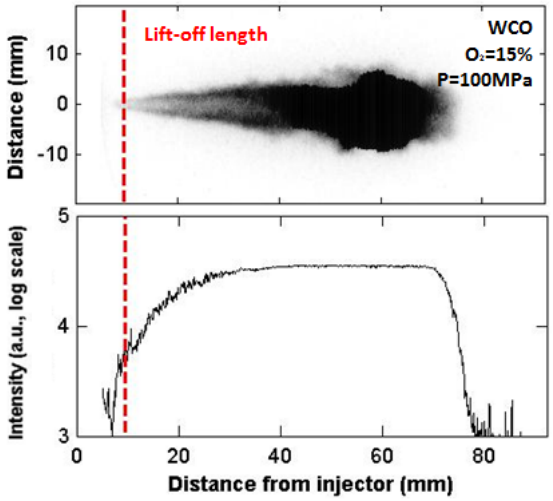

Figure 2: An example of the time-averaged OH-chemiluminescence emission image at 310 nm (top) and its axial intensity profile (bottom). WCO biodiesel was injected at 15 vol.% ambient O_2 concentration and 100 MPa injection pressure by a fuel injector with 105 µm nozzle orifice diameter.

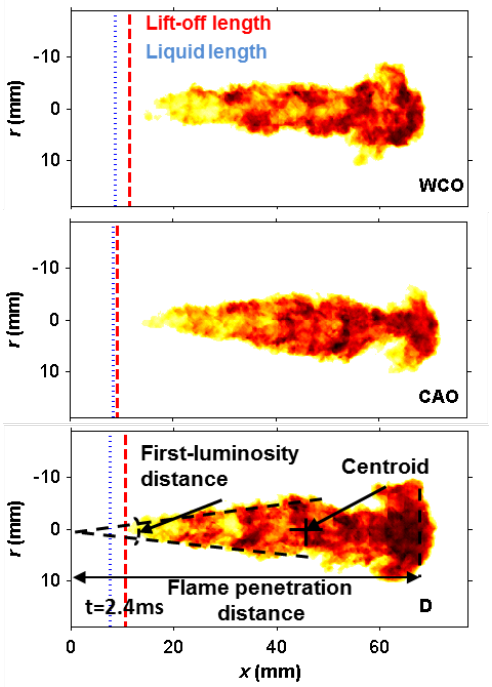

Figure 3: Typical instantaneous flame luminosity images of WCO (top), CAO (middle) and diesel (bottom), recorded at 2.4 ms after SOI at 15 vol.% ambient O_2 concentration and 100 MPa injection pressure. The lift-off lengths and liquid lengths of the flames are indicated using dashed lines. Definitions of centroid, flame penetration distance and first-luminosity distance are also provided in the figures.

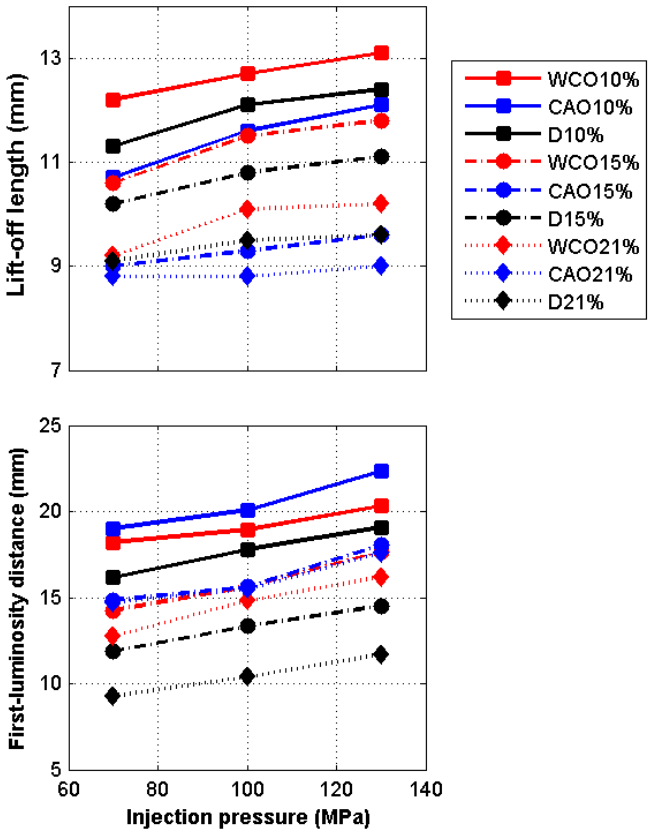

Figure 4: Comparisons of the lift-off lengths (top) and the first-luminosity distance (bottom) of waste cooking oil (WCO), canola oil (CAO) and diesel (D) jet flames. The lift-off lengths and the first-luminosity distances are plotted as functions of injection pressures for three selected ambient O_2 concentrations of 10, 15 and 21 vol.%.

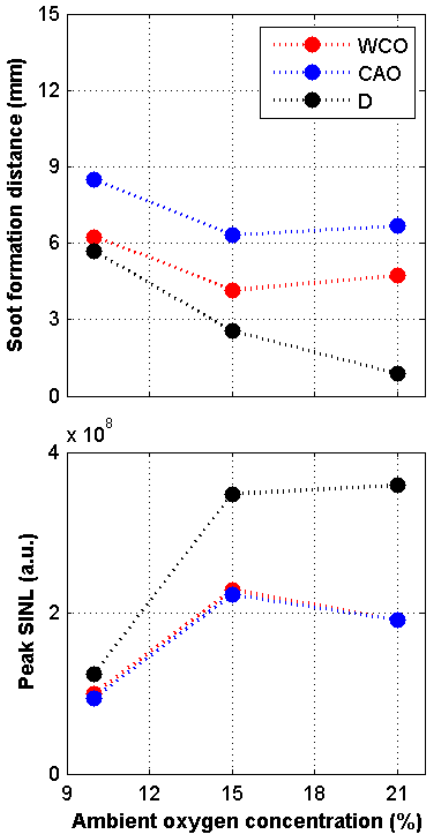

Figure 5: Comparisons of the soot formation distances (top) and the peak SINL (bottom) of waste cooking oil (WCO), canola oil (CAO) based biodiesels and diesel jet flames. The soot formation distances and the peak SINL are plotted as functions of ambient O_2 concentrations, at an injection pressure of 100 MPa.

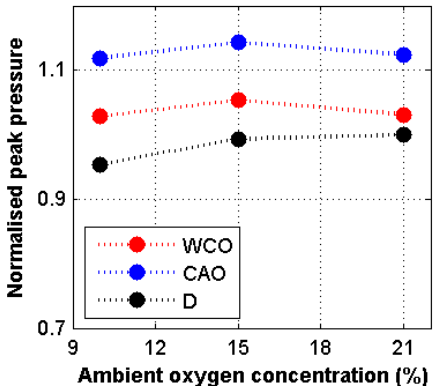

Figure 6: Normalized peak pressures of waste cooking oil (WCO) based biodiesel, canola oil (CAO) based biodiesel and diesel (D) flames, plotted functions of ambient O_2 concentrations, at an injection pressure of 100 MPa.

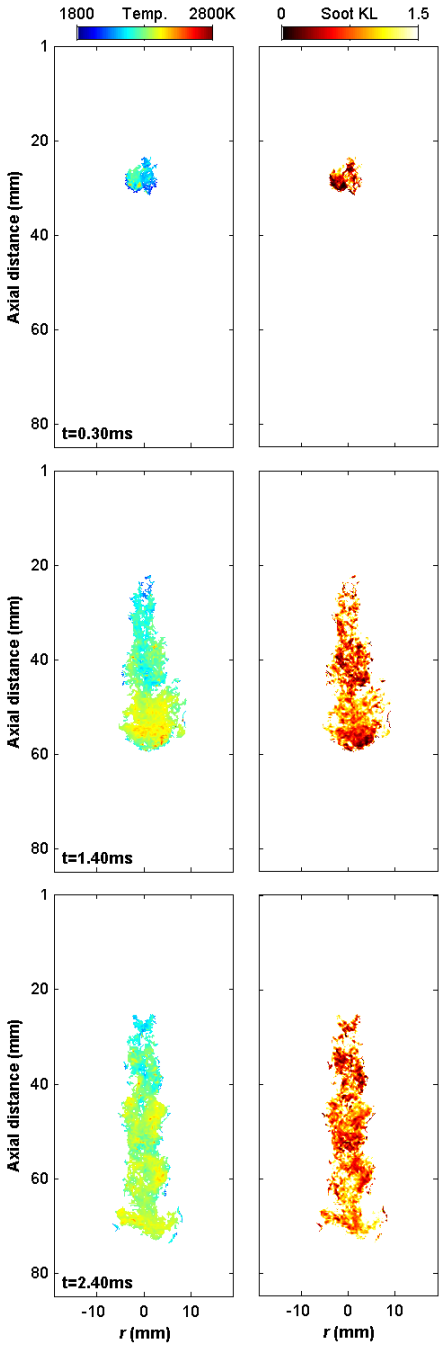

Figure 7: Typical instantaneous two-color soot temperature (left) and KL factor (right) of waste cooking oil biodiesel combustion under 15% O_2 condition. The fuel is injected from the top to bottom, in these images.

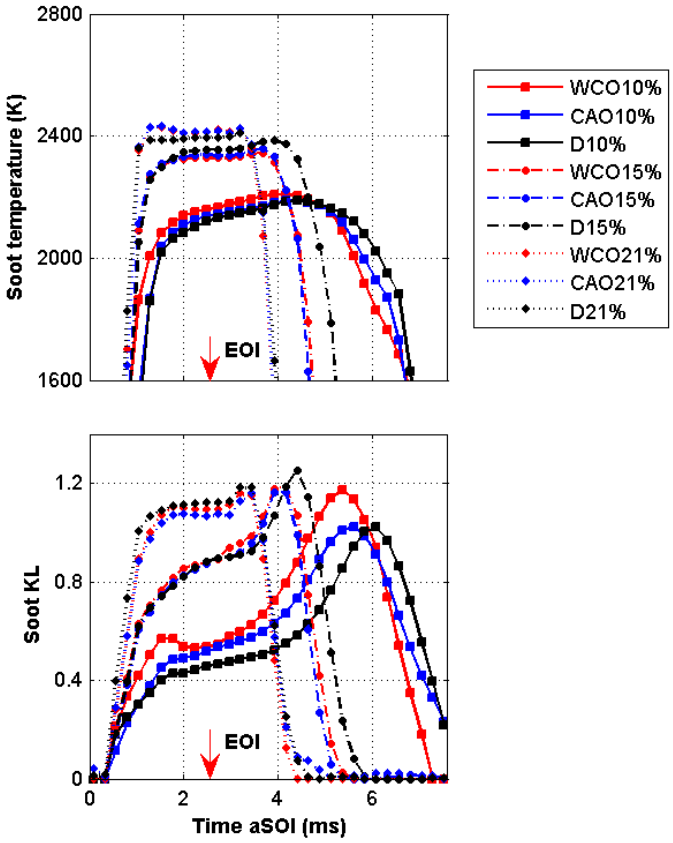

Figure 8: The time-resolved results for pixel-averaged soot two-color temperature (upper) and soot KL factor (lower) for waste cooking oil (WCO) based biodiesel, canola oil (CAO) based biodiesel and diesel (D), plotted as functions of ambient O_2 concentrations, at an injection pressure of 100 MPa. The timing of the end of injection (EOI) is indicated on the plot.

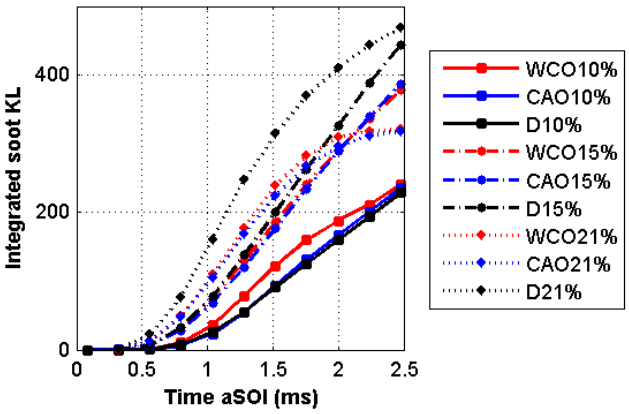

Figure 9: The time-resolved spatially-integrated soot KL factor (lower) for waste cooking oil (WCO) based biodiesel, canola oil (CAO) based biodiesel and diesel (D), plotted as functions of ambient O_2 concentrations, at an injection pressure of 100 MPa.